Comparison of Measured Model and Theoretical Structural Response to Sinusoidal Excitation Pulses

Eric Diels

Northwestern University
Evanston, IL

Introduction and Abstract

A three story, three degree-of-freedom, model structure with a floor width to height ratio of approximately 3:2, shown in Figure 1, was excited with two types of repetitive horizontal motion. One was produced by a programmable shake table—shown supporting the structure in Figure 1a—and produced a reasonably sinusoidal input displacement pulse. The other was produced with an electric motor rotating a mechanical eccentric cam, shown in Figure 1b. While the excitation displacement lf the motor-cam system was far from sinusoidal, it was able to produce sinusoidal structure response because of its repetitively uniform nature. The motor and cam's input frequency was manipulated to excite the model at its first, second, and third modes of response. The shake table's input frequency was controlled to excite the model at frequencies deviating 2.5, 5, and 10 % from the natural or fundamental frequency. The shake table produced a more controllable and more perfectly sinusoidal excitation motion. The shake table was only capable of excitation motions of up to 5 Hz, and thus the motor-cam system was employed to observe model response at it higher modes of response at 5.55 and 8.33 Hz.

This paper compares horizontal velocity and displacement responses measured with velocity transducers (geophones, shown in Figure 1) with theoretical displacement response as well as the shape of the theoretically expected deflected floor displacements at the first, second, and third modes of response. In addition, this paper describes use of velocity transducers to measure response at frequencies below their linear range as well as challenges of comparing mathematical theory to actual measurements for a small number of sinusoidal excitation pulses. Finally, suggestions are given for future use of this model system and shake table for measurement of column strains and excitation at higher frequencies and transient pulses.

Equipment and Instruments

The apparatus has two configurations shown in Figure 1a and 1b. Both consist of three main components: a model structure, a device to excite the model, and velocity transducers to capture the model's motion. For structural excitation, a shake table and an electric motor-cam system were used, shown in Figure 1a and 1b, respectively.

The model structure features all-metal construction with thin, flexible walls and thick, relatively more massive floors. Approximately 21 cm separate each floor, and floors are 30 cm wide. With three floors above ground level, this model acts as a three degree-of-freedom system with three masses of the same weight at each floor.

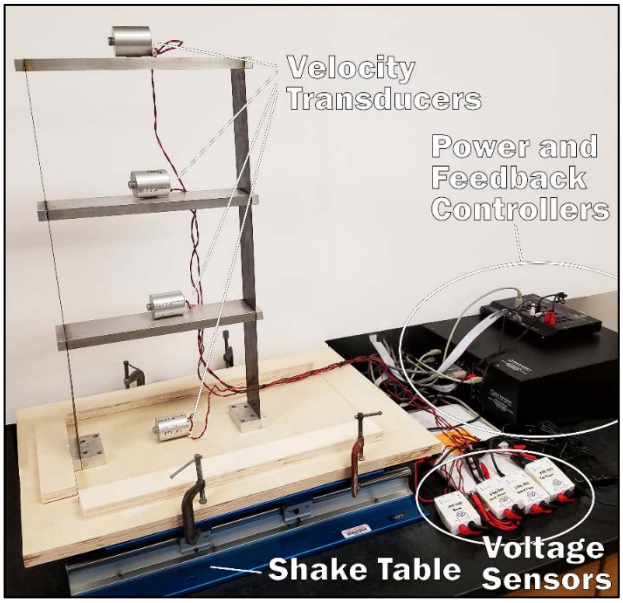

Figure 1a: The testing apparatus consisting of the model structure, input device (here the Shake Table II), and recording devices (velocity transducers recorded by voltage sensors).

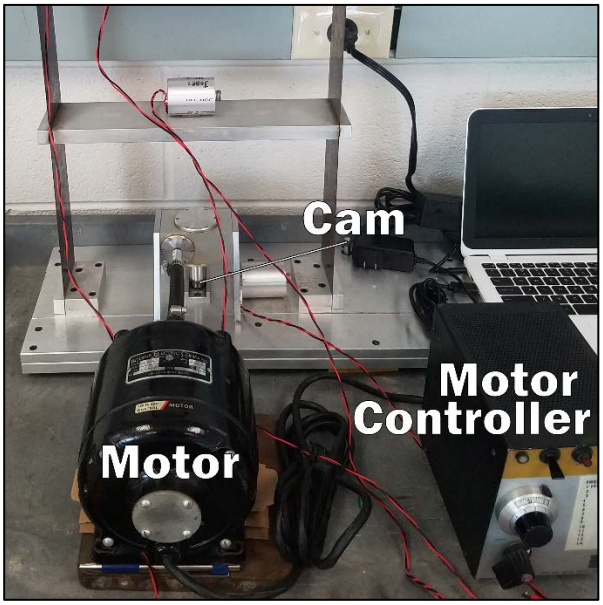

Figure 1b: The alternative apparatus configuration using a motor and cam system to excite the model structure.

In the first configuration, structural excitation was provided by the Quanser Shake Table II, shown in Figure 1a. According to Quanser, this shake table is rated to drive a 7.5 kg load at 2.5 g and has a maximum displacement of ± 7.62 cm (Quanser, 2017), far above requirements necessary for this research. Power and feedback controllers—along with manufacturer provided control software—direct the shake table's movements. This software provides amplitude and frequency control of a sinusoidal time-displacement function used to excite the model structure. For this configuration, the model was screwed to a wooden platform, allowing it to be clamped securely to the shake table.

Structural excitation was provided by a motor-cam system—shown in Figure 1b—in the second configuration. The motor used was a Bodine Electric Company Series 500 Control Motor. In this configuration, the model structure was screwed to a metal base plate and able to move laterally with little friction. Motor rotation about a horizontal axis was transferred through two conical gears to an eccentric cam rotating about a vertical axis. Rotation of this eccentric cam produced horizontal excitation at the base of the structure. A motor controller was used to adjust the frequency of base excitation.

Input excitation and structural response was captured with Geospace Technologies HS-1 geophones (velocity transducers). These sensors produce an analog voltage related directly to their excitation velocity. Pasco wireless voltage sensors measured the transducer's analog voltage signal and relayed it digitally to Pasco's Capstone software to record voltage time histories. Voltage data were then converted to units of velocity after special calibration described below.

Velocity Transducer Calibration Process

Conversion from velocity transducer output voltage to units of velocity is dependent on the excitation frequency experienced by the transducer. The manufacturer provided conversion chart (upper right portion of Figure 2) displays nonlinear response below 20 Hz and does not extend below 5 Hz. Because the first three excitation modes of the structure (1.91, 5.55, and 8.33 Hz) occur below the flat response region, and the fundamental mode frequency (1.91 Hz) does not appear on the manufacturer conversion chart, it was necessary to manually calibrate voltage-to-velocity conversion rates. These calibrated conversion rates are labeled in Figure 2 for the first three excitation modes.

Accurate conversion rates make it possible to calculate true velocity and displacement data. Conversion rates calculated during this research deviated from the manufacturer calibration chart. The dashed red line in Figure 2 is an extension of the manufacturer provided curve—assuming it continues linearly. Calibrated conversion rates for each of the three excitation modes lie above the manufacturer curve. Furthermore, while these points are not consistent with manufacturer expectations, they follow a linear relationship.

Velocity transducers were calibrated through a multistep process. First the structure's fundamental frequency was found. To do so, an assumption was made: maximum structural response occurs when base input frequency matches the structure's fundamental frequency. Therefore, by trial and error, base input frequency was adjusted, searching for maximum structural response. Once this frequency was found, it was considered the structure's fundamental frequency. Structural response was observed by monitoring output voltage amplitude—no conversion factor necessary since velocity varies directly with output voltage.

The next step of calibration was recoding structural excitation at its fundamental frequency independent of the velocity transducers by visually measuring the displacement. First, a ruler was placed behind the top floor, as shown in Figure 3. Then the structure was excited with a base input frequency equal to its calculated fundamental frequency, and voltage time histories were recorded. When the top floor transducer's output voltage amplitude reached a steady maximum, a video of the top floor moving relative to the ruler was recorded to measure displacement at the top floor.

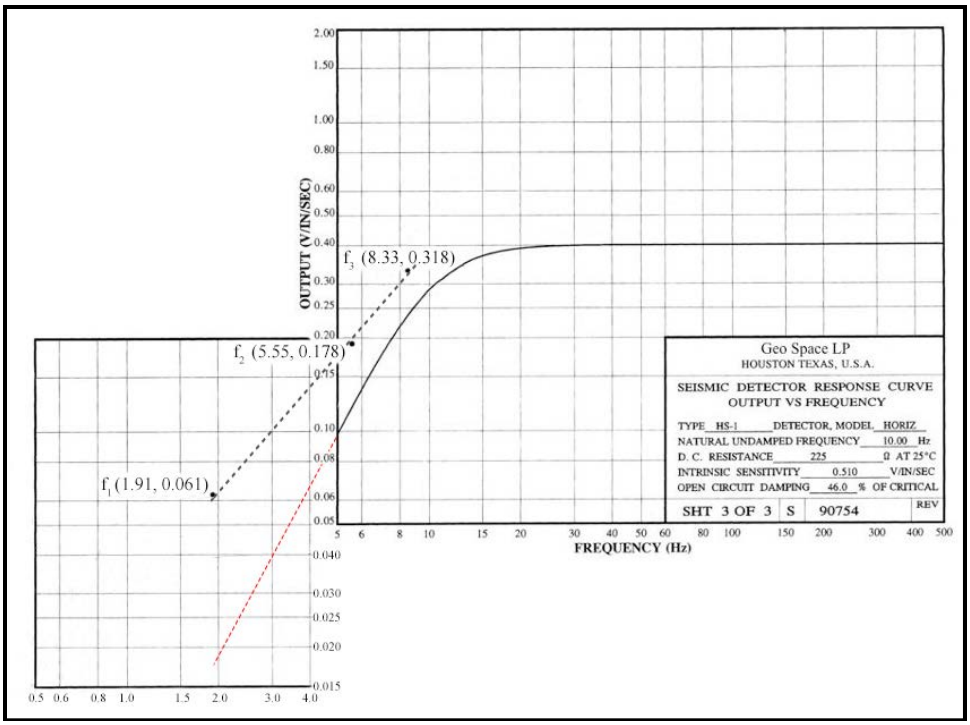

Figure 2: The upper right portion of the velocity transducer conversion chart is taken directly from the velocity transducer manufacturer (HS-1). On the lower left in red is a theoretical linear extension of the manufacturer given conversion chart. The three points—f_1, f_2, and f_3—represent conversion rates calculated during testing at the structure's first, second, and third excitation modes, respectively.

Figure 3: A ruler positioned behind the top floor determined maximum displacement during excitation. This displacement was then used to manually calculate the velocity transducer conversion rate.

The last step of velocity transducer calibration was data analysis. Video of the shaking structure provided the maximum displacement during steady-state fundamental frequency excitation. Using Figure 2, an initial voltage-to-velocity conversion rate was selected to calculate velocity, which was subsequently integrated to calculate displacements (example time histories shown in Figure 4). Amplitude of this displacement at steady-state was then

compared to maximum displacement found from video analysis. To find the correct conversion rate, the voltage-to-velocity conversion rate was adjusted manually until displacements calculated from velocities matched those from video analysis. This final conversion rate was considered the true, calibrated conversion rate and was used for the rest of analysis. To calculate the voltage-to-velocity conversion rates for the second and third mode frequencies, this process was repeated.

Shake Table Base Input Velocity and Displacement Limitations

Though the Shake Table II is a well-developed instrument useful for applications in engineering research, physical limitations mean the system will never produce perfect movements like those assumed in mathematical models. In particular, the shake table's displacement is not purely sinusoidal and takes a non-negligible amount of time to reach steady-state. Examples of input velocity and displacement time histories are shown in Figure 4a and 4b.

Input velocity, shown in Figure 4a, is obviously not a clean sinusoidal function; however, a 50-period moving average (equating to 0.1 seconds at a recording rate of 500 Hz) illustrates the velocity is nearly sinusoidal *on average*. Shown in Figure 4b, input displacement is more sinusoidal than velocity but still not perfectly sinusoidal. Nevertheless, structural response at the top floor—velocity and displacement shown in Figures 4c and 4d, respectively—*is* sinusoidal. Thus, because the structural response was sinusoidal as expected, the imperfect base input displacement was deemed acceptable for this research.

Velocity and displacement of the shake table also cannot reach steady-state amplitudes instantaneously: a short period of "initiation" time is necessary to allow the system to reach the required frequency starting from a fixed position (or "zero" frequency). The black box in Figure 4b outlines this time of system "initiation." Because pulses from the shake table do not begin at steady-state amplitude, it is difficult to determine which is the "first" pulse exciting the structure. For the purposes of this paper, the first excitation pulse refers to the first input pulse reaching steady-state amplitude.

Motor-Cam Base Input Velocity and Displacement Limitations

The motor and cam system configuration is a rather simple mechanical system—less the electric motor, of course. However, like the shake table, input displacements produced by the motor and cam are not purely sinusoidal. Examples of input velocity and displacement time histories are shown in Figure 5a and 5b.

Another limitation of the motor and cam system is consistency of excitation frequency. Unfortunately, the motor cannot reliably produce the same driving frequency by setting the motor control to a known position; input frequency is only accurately known at steady state when structural response is at a maximum. Therefore, increasing response to

excitation pulses cannot be measured with the motor and cam system: only steady-state excitation is possible.

Input velocity, shown in Figure 5a, is certainly not a clean sinusoidal function; even a 50-period moving average (equating to 0.1 seconds at a recording rate of 500 Hz) does not help the input appear much more sinusoidal. Input displacement, shown in Figure 5b, is more sinusoidal than velocity; however, it is still not perfectly sinusoidal. It also does not have a constant average value but instead "wanders" up and down in amplitude. Even so, structural response at the top level—velocity and displacement shown in Figures 5c and 5d, respectively—*is* sinusoidal. However, like with the shake table, structural response was sinusoidal as anticipated, therefore this imperfect base input displacement was considered acceptable.

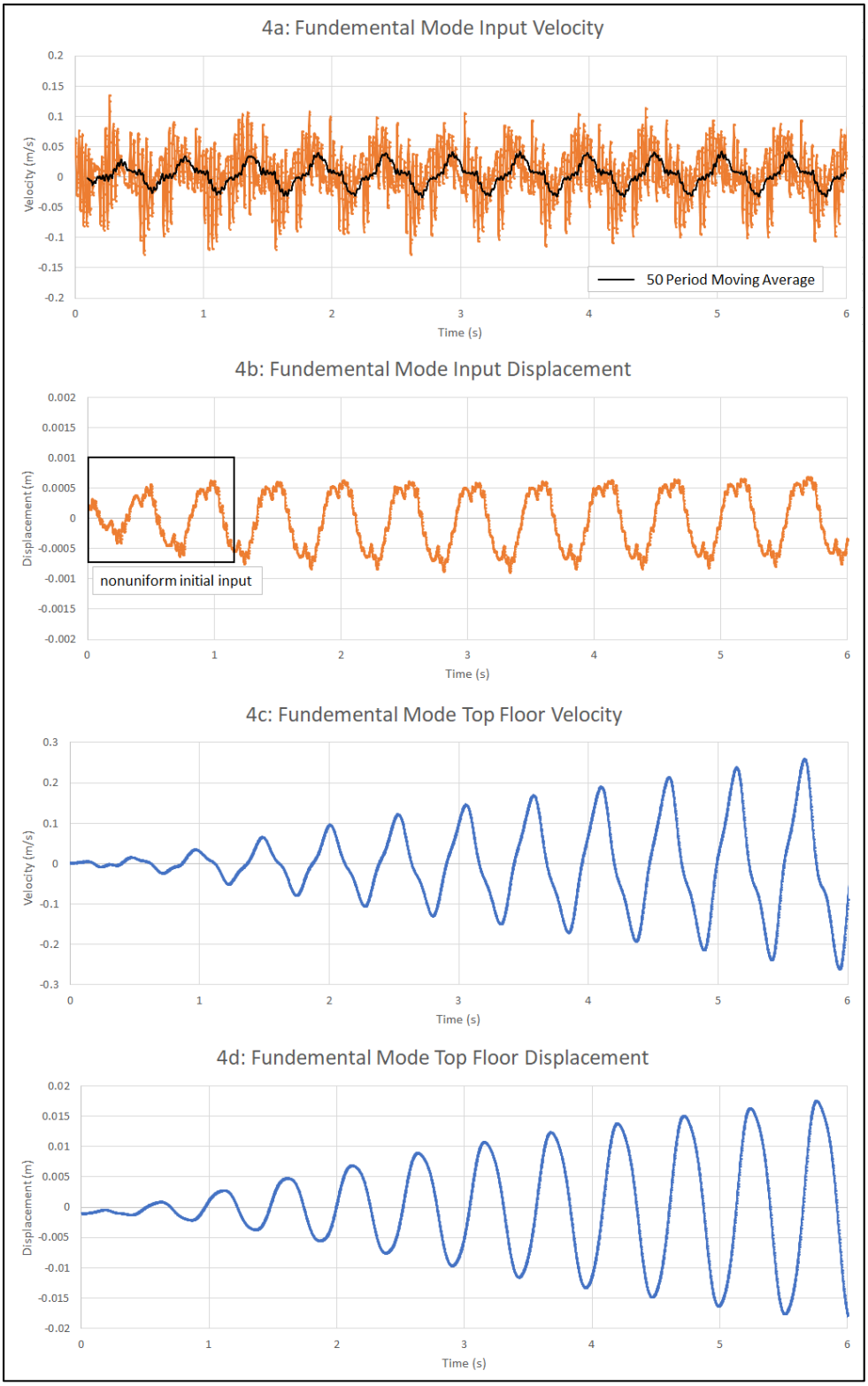

Figure 4: Example of the velocity and displacement time histories—recorded at the fundamental mode of the model structure with the shake table as the driving device. While the input velocity is noisy, the input displacement is cleaner, and the top floor velocity and displacement appear to be much cleaner sinusoidal responses. The black box highlights time needed for base input to "initiate" itself to steady state amplitude.

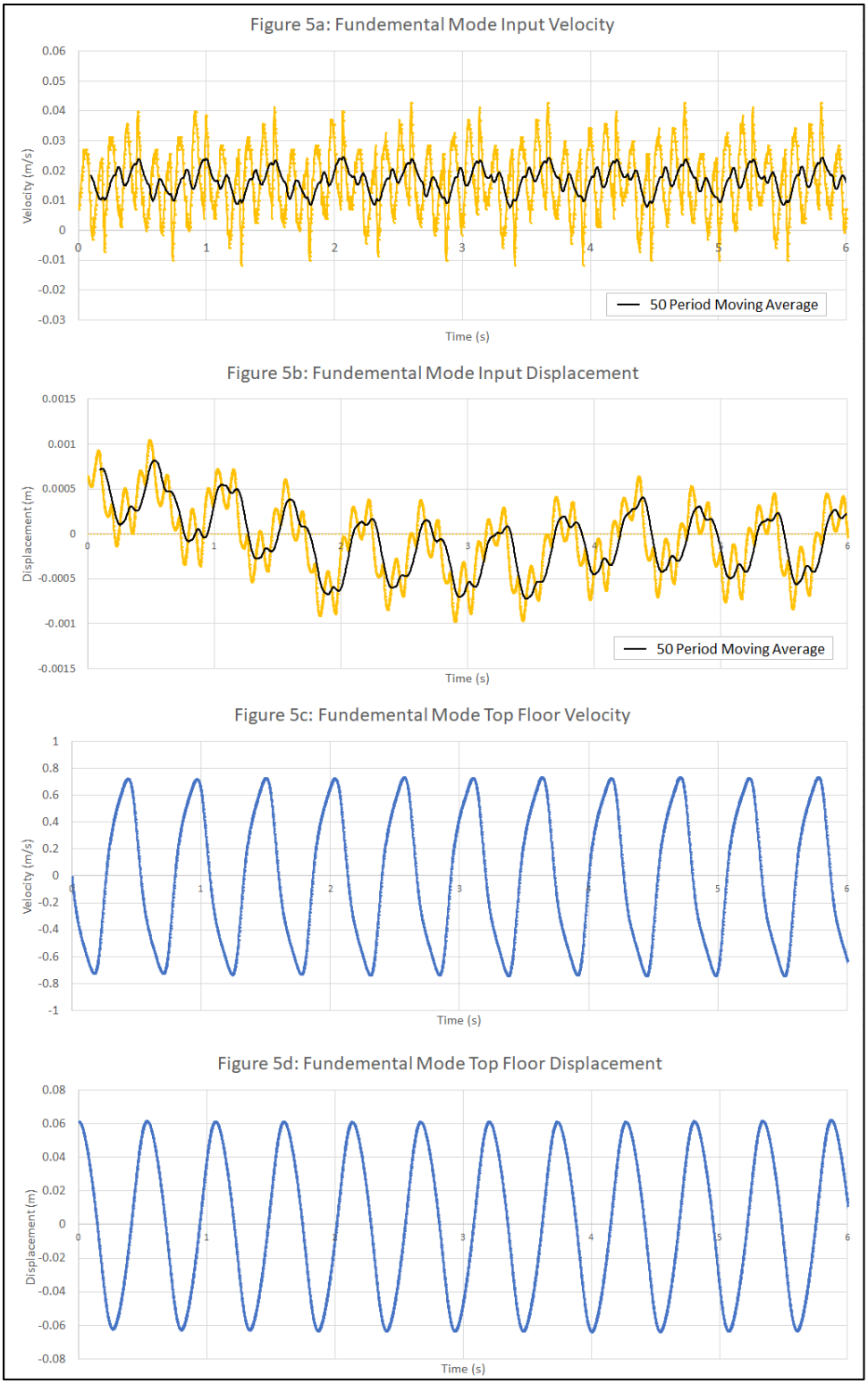

Figure 5: Example of the velocity and displacement time histories—recorded at the fundamental mode of the model structure with the motor and cam system as the driving device. Input velocity and displacement are very noisy, but the top floor velocity and displacement appear to be much cleaner sinusoidal responses. Fifty period moving averages demonstrate the periodic nature of input excitation.

Model Structure Excitation Mode Frequencies

Fundamental (first), second, etc. modes of structural response can be estimated for any body or structure. For example, a continuous body of soil with distributed mass has multiple modes of shear response described by Equation 1.

$$\omega_n = \frac{v_s}{H}\left(\frac{\pi}{2} + (n-1)\pi\right) \quad (1)$$

Here, v_s is the shear wave velocity, H is the height of the soil deposit, and $n = 1, 2, 3, \ldots$ is the mode number (Kramer, 1996). Thus, the first three mode frequencies are

$$\omega_1 = \frac{\pi v_s}{2H} \text{ for the fundamental (first mode),}$$

$$\omega_2 = \frac{\pi v_s}{2H} + \frac{v_s \pi}{H} = 3\omega_1 \text{ for the second mode,}$$

$$\text{and } \omega_3 = \frac{\pi v_s}{2H} + \frac{2 v_s \pi}{H} = 5\omega_1 \text{ for the third mode.}$$

Similarly, a lumped body system like a multilevel structure also has multiple modes of horizontal (or shear) response. For instance, Mncwango (1990) used Equation (2) for multiple modes of response for an N degree-of-freedom system, that is, a structure with N floor levels.

$$\omega_j = 2\sqrt{\frac{k}{m}}\sin\left(\frac{(2j-1)\pi}{2(2N+1)}\right) \quad (2)$$

In this equation, $j = 1, 2, 3, \ldots$ is the mode number, m is the mass, and k is the stiffness. Using structural properties of $m = 118.8\ kips$ and $k = 109.389\ kips/in$, the model frequencies were $\omega_1 = 18.8486$, $\omega_2 = 52.8212$, and $\omega_3 = 76.3302$. Thus, $\omega_2 = 2.8\omega_1$, and $\omega_3 = 4.0\omega_1$.

Using the method described in the velocity transducer calibration process section, the first three excitation mode frequencies of the structural model were found experimentally. Because the shake table's control software limits sinusoidal frequency to 5 Hz (below the second and third mode frequencies), the motor and cam system was used to determine the second and third excitation mode frequencies, shown in Table 1.

Frequency [Hz]	Model Structure
f_1	1.91
f_2	5.55
f_3	8.33

Table 1: theoretical excitation mode frequencies for the model structure.

The ratio of second and third mode excitation mode frequencies to their corresponding fundamental mode frequency are shown in Table 2 for each theoretical and experimental system. Experimental results from the model structure are right between the two theoretical predictions. Because the model structure behaves somewhere between a distributed and lumped mass system, these results are reasonable and provide evidence these experimental results are indeed accurate.

Frequency [Hz]	Distributed Mass	Lumped Mass System	Model Structure
f_2/f_1	3.0	2.8	2.9
f_3/f_1	5.0	4.0	4.4

Table 2: Ratios of second and third excitation mode frequencies to their corresponding fundamental mode frequency for distributed mass (soil) systems, lumped mass (multilevel structure) systems, and the model structure.

Model Structure Damping

No structure is undamped: critical damping of an oscillating structure is calculated from the decay of free oscillation of the structure. After an initial excitation—say, from the push of a finger for a model structure—the resulting declining velocity amplitudes provide data necessary to calculate the system's damping factor, β, from Equation 2 (Dowding, 2000). Here, u_n and u_{n+1} are consecutive velocity amplitudes.

$$\beta = \frac{1}{2\pi}\left(-\ln\left(\frac{u_{n+1}}{u_n}\right)\right) \qquad (2)$$

Figure 5 illustrates the decay in velocity during free oscillation of the model structure. The damping factor was calculated to be $\beta \approx 2$ % indicating a relatively undamped structure.

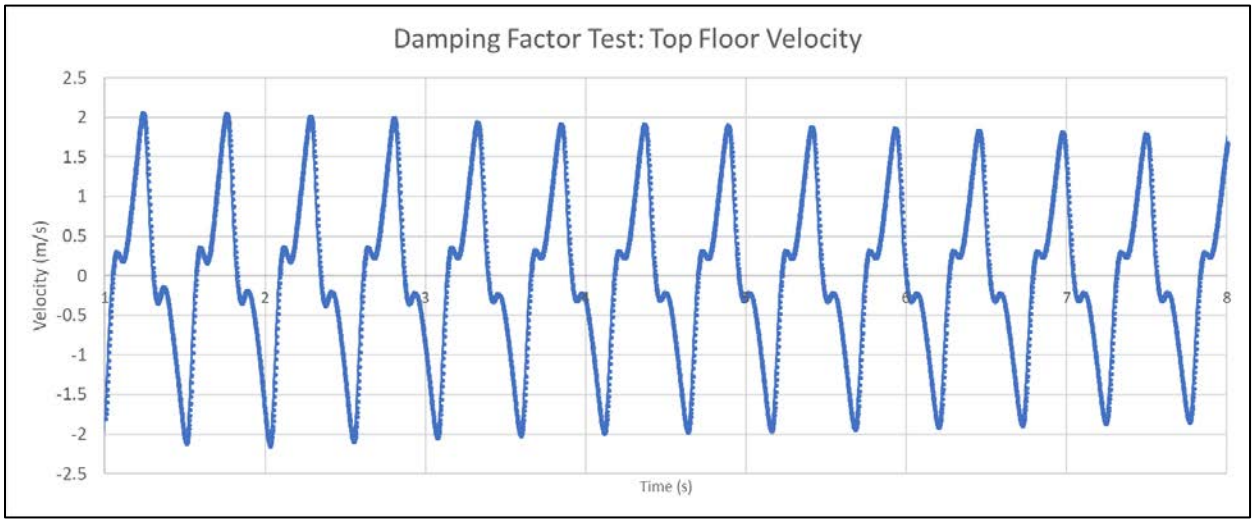

Figure 5: Top floor velocity time history during damping factor, β, calculation test showing the decay of free oscillation. The velocity amplitudes are used to calculate the damping factor of the structure.

Structural Response to Increasing Numbers of Constant Amplitude Excitation Pulses

Continued exposure to base motion produces increasing structural response. Figure 6 illustrates this increasing response amplitude for both measurement of model response (experimental) and mathematical calculation (theoretical). With damping at 2 %, experimental and theoretical results for base input at the fundamental frequency are remarkably similar—both increase to just under a dynamic amplification factor (DAF) of 20 at 12 pulses.

The rigorous definition of the DAF is observed displacement induced by the peak of the exciting force divided by static displacement. However, since the exciting force is not known, the displacement observed after one pulse has been employed as the equivalent static displacement. Measured DAF was obtained by dividing the displacement after each pulse by the first pulse and them multiplying by the DAF for one pulse found in Mncwango's thesis.

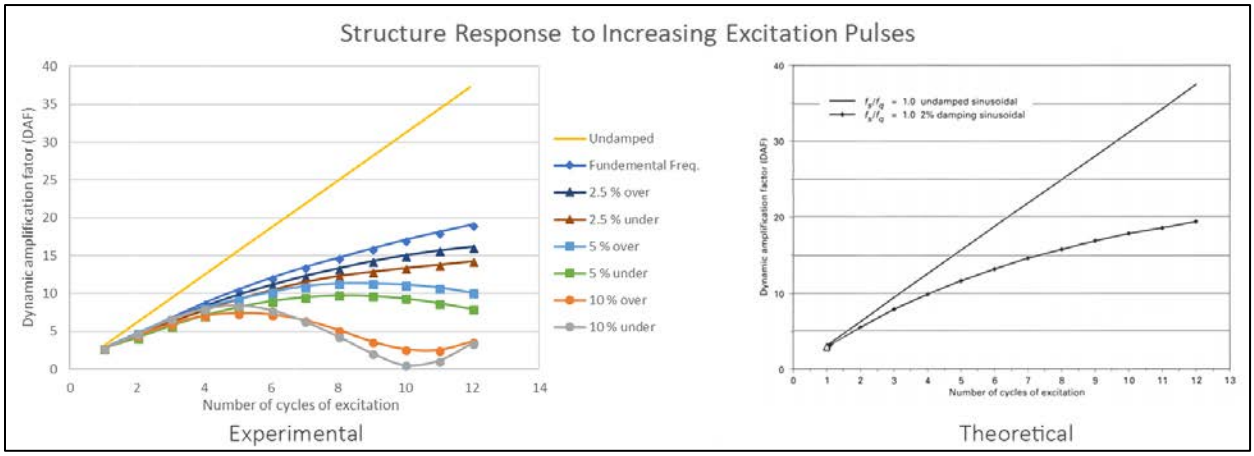

Figure 6: Structural response to increasing number of excitation pulses—calculated and theoretical (Mncwango, 1990) values. Input frequencies of 10, 5, and 2.5 % over and under the fundamental frequency are shown in addition to the fundamental frequency for the calculated chart.

Experimental response to continuous excitation pulses at the structure's fundamental mode was remarkably similar to Mncwango's mathematical theorization. Thus, the mathematical model confirms the validity of this experimental model.

The experimental plot in Figure 6 also displays structural response for input frequencies deviating from the fundamental frequency. If the base input frequency matches the structure's fundamental frequency exactly, structural response will increase asymptotically to steady state excitation. However, if the base input frequency deviates from the fundamental frequency, structural response experiences oscillating amplitude over time, whose maximum is less than at the fundamental frequency. An example is shown in Figure 7; here, input frequency was 10 % above the fundamental. Oscillation occurs as base input and structural response move in and out of phase. While structural response is increasing,

base excitation closely coincides with structural response. Structural response declines as the excitation pulse opposes structural response.

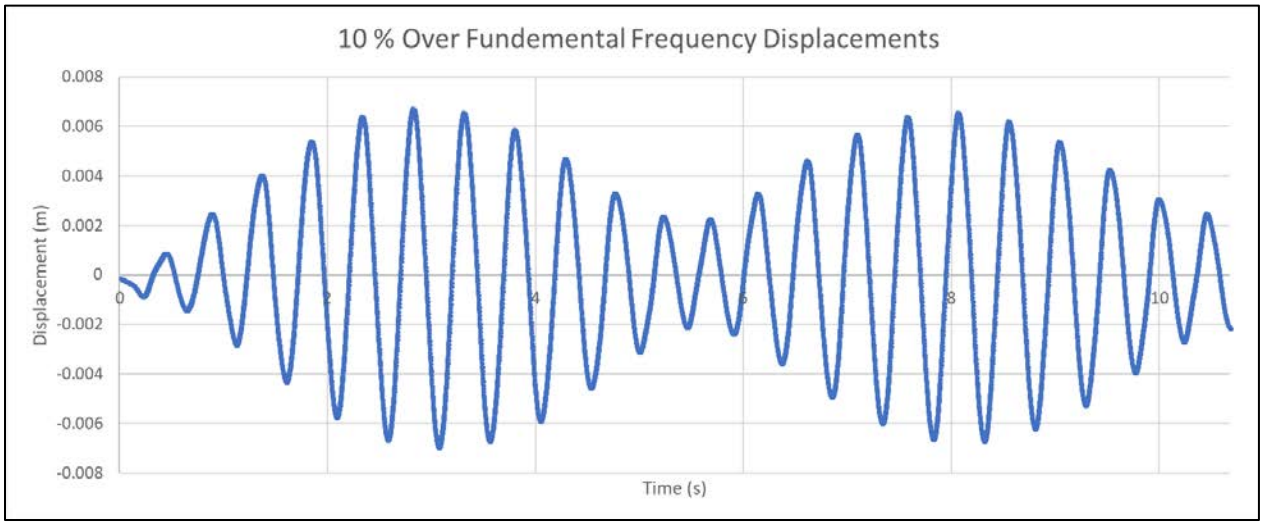

Figure 7: Input frequencies deviating from the fundamental frequency—in this case, 10 % over—demonstrated periodic response cycles.

Maximum Structural Response During Excitation

Inter-story drift for each excitation mode is shown in Figure 8 and 9. Displacement at each story is normalized to the largest displacement at that excitation frequency in Figure 8. This method illustrates the relative displacement between each story but exaggerates the actual displaced shapes when comparing excitation modes. Contrarily, in Figure 9, displacement at each story is normalized to the largest displacement at any of the three excitation frequencies (occurring at the top floor at the fundamental frequency). This method illustrates relative deflection curves for each excitation mode, allowing excitation mode displacements to be compared with one another.

Actual maximum displacements after 12 pulses at the fundamental mode for experimental and theoretical models were 2.0 cm and 16.9 cm respectively. The maximum theoretical displacements are far larger because the theory modeled a full-scale, real structure while experimental displacements were for a 0.6 m tall model. However, while actual deflections differ, the shape of their relative displacements can still be compared to validate achievement of second and third mode response for the model.

In both Figure 8 and 9, Mncwango's mathematical results are also shown beside their corresponding experimental results. The deflected shape from experimental measurements and Mncwango's theoretical calculations showed similarities. At each excitation mode, each approach found the same floor level with maximum displacement and also had the same general deflected shape.

There were differences between experimental and theoretical calculations, however. For example, as shown in Figure 9, experimental relative displacement between stories

deviated from theory more for the higher modes, the second and third. Possible sources for this error include differences between the experimental and theoretical structures' wall stiffness values, floor height to width ratios, and support conditions.

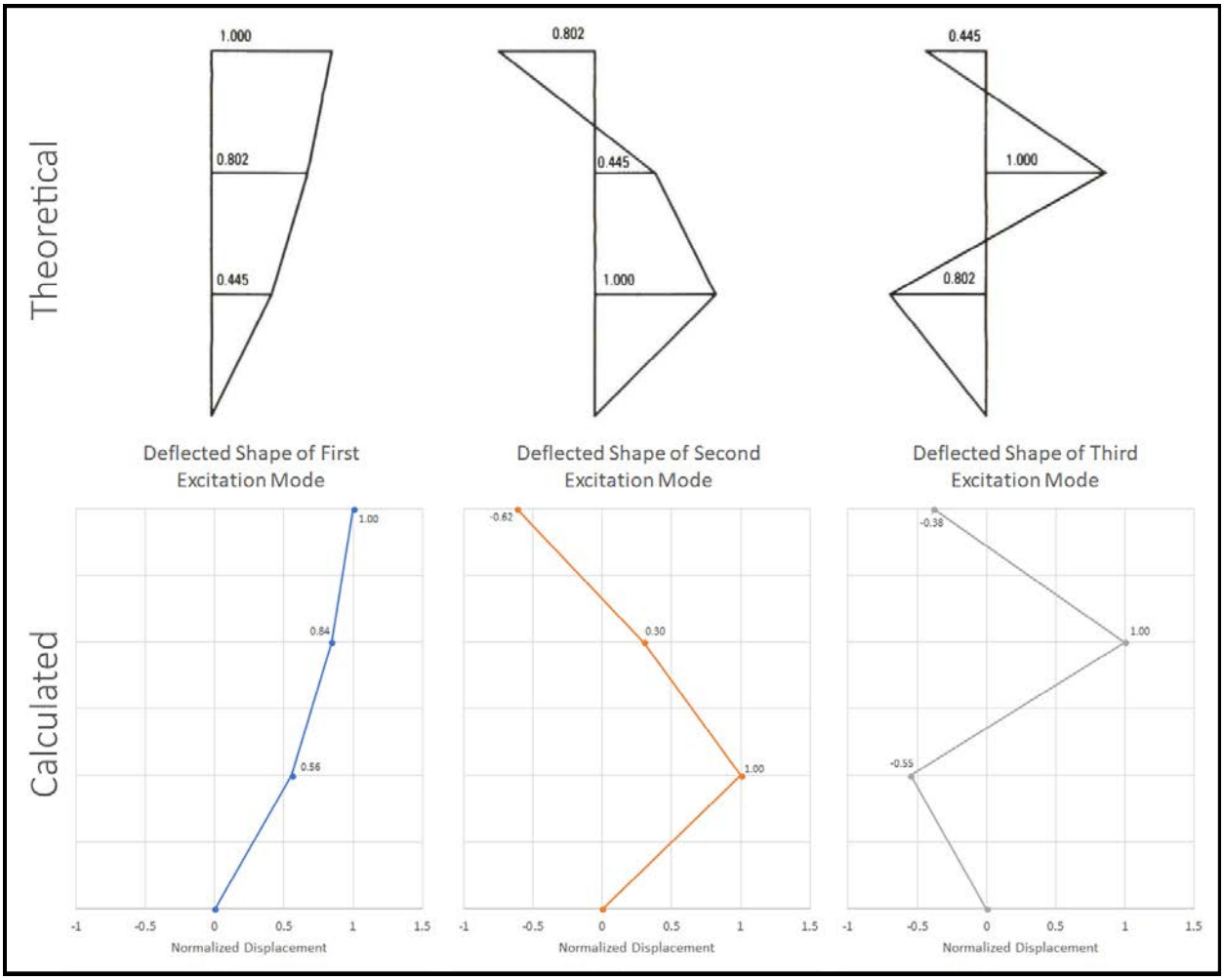

Figure 8: Theoretical (top) (Mncwango, 1990) and calculated displacement (bottom) at each floor normalized to the largest displacement of the three floors. These plots show the structure's deflected shape during excitation at the first three modes.

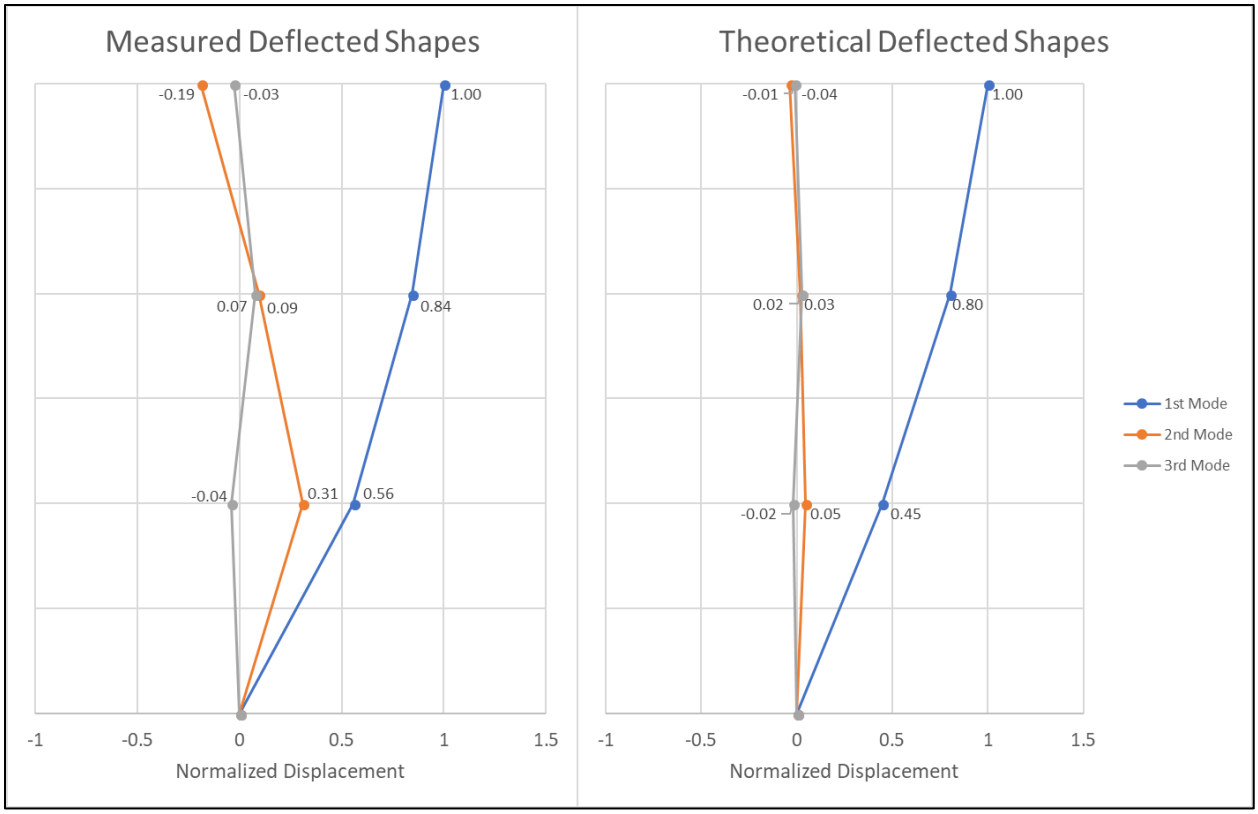

Figure 9: Comparison of experimental and theoretical (Mncwango, 1990) deflection during first, second, and third mode excitation. Note that the magnitude of deflection decreases with increasing frequency.

Finally, deflection shape details produced at the fundamental frequency is captured visually in Figure 10. This photo confirms the deflected shape found theoretically and experimentally through velocity integration. Furthermore, the shape of the model's walls during horizontal model defection indicates a tendency toward fixed-fixed support conditions between floors.

Figure 10: A photograph of the structure's deflected shape during fundamental frequency excitation. The columns exhibit fixed-fixed support behavior.

Conclusions and Recommendations for Further Research

Comparison of theoretical results from Mncwango's mathematical building model and experimental measurements of the response of a model structure tested the validity of the experimental model. Results from this experiment closely paralleled Mncwango's mathematical approach. Therefore, this model structure may indeed be a reliable approximation of structural behavior.

Inter-story wall deflection for this model structure tended toward a fixed-fixed support condition. For future research, strain gages may be added to the walls. Strain from these gages could then be compared to theoretical strain calculated from inter-story drift and this fixed-fixed support assumption.

Because the shake table is more convenient to operate than the motor and cam and provides more predictable results, utilizing the correct software to excite the structure at higher modes would be beneficial for reproducing these experiments. Additionally, programming the shake table to excite the structure with a transient (i.e. noncontinuous) pulse would facilitate investigation of structural response to a fixed number of pulses instead of continuous motion, as well as odd shaped single transients similar to those produced blasting and construction.

References

Dowding, C. H. (2000). Construction Vibrations. Prentice Hall, Upper Saddle River, NJ.

"HS-1 Industrial Geophone." (n.d.). Geospace Technologies, <https://www.geospace.com/sensors/hs-1/> (May 30, 2018).

Kramer, S. L. (1996). *Geotechnical Earthquake Engineering*. Prentice Hall, Upper Saddle River, NJ.

Mncwango, S. W. (1990). "Finite Pulse Excitation Models for Blast Excitation." thesis.

Quanser Inc. (2017). "Shake Table II User Manual." Shake Table II User Manual, Quanser Inc., Markham, Ontario.